# Time-Dependent Schrödinger Equation using the Space Discretized Leapfrog Technique

Andrew Hayman[1,*]

[1] *Department of Physics, Engineering Physics and Astronomy, Queen's University, Kingston, ON K7L 3N6, Canada*

(Dated: February 13, 2022)

The famous Time-Dependent Schrödinger Equation (TDSE) is a fundamental quantum mechanical equation that governs the evolution of a quantum wave function. Solving the TDSE analytically is possible only for the simplest Hamiltonians, making numerical methods critical for more complex and realistic cases such as molecular dynamics. Here, we apply the space discretized Leapfrog technique to solve the TDSE for three potentials: a free particle, a harmonic oscillator, and a double-well potential. We recover the expected behaviour in all cases. The free particle demonstrates dispersion, the harmonic oscillator demonstrates oscillatory motion, and the double-well demonstrates periodic quantum tunneling across the two wells. The Virial theorem is verified for the harmonic oscillator, and the coefficients of the double-well are compared against the quantum tunneling period. Finally, we compare full matrix multiplication, sparse matrix multiplication and matrix slicing for solving the equations of motion and demonstrate that matrix slicing is around 2.4 times faster than sparse matrix multiplication, and that both sparse and slicing vastly outperform full matrix multiplication.

## I. INTRODUCTION

The Time-Dependent Schrödinger Equation (TDSE) is a fundamental quantum mechanical equation that describes the evolution of a quantum state's wave function. Most applications involving quantum mechanics rely on the TDSE such as quantum computing, optical pumping, molecular dynamics, quantum chemistry and more. The TDSE is completely deterministic. The wave function can be calculated at any point in time knowing the initial conditions and boundary conditions. However, this is challenging to calculate analytically beyond the simplest Hamiltonian, so numerical methods are critical for more complex, realistic cases.

Here, we investigate the Hamiltonians of particles in three different potentials using the numerical the space discretized Leapfrog technique. We examine a particle in free space, in a harmonic oscillator and in a double-well potential using a Gaussian function as the initial wave packet. In each case, we use animations to examine the evolution of the wave function. Here, we show snapshots of the wave function animations, as well as probability density functions. For the case of free space, we compare the full matrix multiplication, sparse matrix multiplication and matrix slicing for solving the equations of motion to identify the fastest method of computation. For the harmonic oscillator, we demonstrate that the Virial theorem is satisfied using numerical differentiation and integration. Finally, for the double-well potential, we investigate the rate of quantum tunneling based on the potential's coefficients.

## II. THEORY AND EQUATIONS

The TDSE describes the evolution of a the wave function of a quantum state in one dimension by

$$-\frac{\hbar^2}{2m}\frac{\partial^2\psi(x,t)}{\partial x^2} + V(x,t)\psi(x,t) = i\hbar\frac{\partial\psi(x,t)}{\partial t}. \quad (1)$$

Reduced units simplify the computational implementation of the TDSE, where $\hbar = m_e = e = 1$ to give

$$-\frac{1}{2}\frac{\partial^2\psi(x,t)}{\partial x^2} + V(x,t)\psi(x,t) = i\frac{\partial\psi(x,t)}{\partial t}. \quad (2)$$

For the remainder of this paper, atomic units will be used. The TDSE is trivial to extend to three dimensions, but for the purpose of the numerical simulations in this paper, only one dimension will be used. The quantum state, $\psi(x,t)$ must be normalized over all time in the Hilbert space, where

$$\int_{-\infty}^{\infty} |\psi(x,t)^2| = 1. \quad (3)$$

The initial conditions and the potential, $V(x,t)$ determine how the state evolves from $t = 0$. Here, we investigate the potential of a free particle where $V(x,t) = 0$, a harmonic oscillator where $V(x,t) = \frac{1}{2}x^2$, and a double-well potential where $V(x,t) = ax^4 - bx^2$.

To evaluate how the state evolves over time, it is useful to consider the probability density and the expectation of observables. The probability density function can be described by

$$PDF(x,t) = |\psi(x,t)^2|. \quad (4)$$

which is subject to normalization describe in Eq. 3. The expectation values of the position, momentum, kinetic energy and potential energy in the x position basis are described by

* 18arth@queensu.ca

$$\langle x \rangle = \int_{-\infty}^{\infty} \psi^*(x,t) x \psi(x,t) dx \tag{5}$$

$$\langle p \rangle = \langle \frac{1}{i}\frac{\partial}{x} \rangle = -i \int_{-\infty}^{\infty} \psi^*(x,t) \frac{\partial \psi(x,t)}{\partial x} dx \tag{6}$$

$$\langle T \rangle = \langle \frac{p^2}{2} \rangle = \frac{1}{2} \int_{-\infty}^{\infty} \left| \frac{\partial \psi(x,t)}{\partial x} \right|^2 dx \tag{7}$$

$$\langle V \rangle = \int_{-\infty}^{\infty} \psi^*(x,t) V(x,t) \psi(x,t) dx. \tag{8}$$

The TDSE can be solved numerically for any potential and initial condition by applying space discretization and a numerical method.

To put the TDSE in a convenient matrix form for numerical methods, we can use space discretization. Let $x_j = jh$ be a discrete position where $j = 0, 1, ..., N$ to get $\psi_j(t) = \psi(jh, t)$ and $V_j(t)$ =V(jh,t). We can then divide the wave function into real an imaginary parts where

$$\psi_j(t) = R_j(t) + iI_j(t). \tag{9}$$

This generates two equations of motion for the wave function:

$$\frac{dR_j}{dt} = -\frac{1}{2h^2} I_{j-1} + \left( \frac{1}{h^2} + V_j \right) I_j - \frac{1}{2h^2} I_{j+1} \tag{10a}$$

$$\frac{dI_j}{dt} = \frac{1}{2h^2} R_{j-1} - \left( \frac{1}{h^2} + V_j \right) R_j + \frac{1}{2h^2} R_{j+1}. \tag{10b}$$

We can then define $a_j = \frac{1}{h^2} + V_j$ and $b = -\frac{1}{2h^2}$, and expand the equations of motion into their matrix form for N discrete steps with

$$\frac{d\mathbf{R}}{dt} = A\mathbf{I}, \quad \frac{d\mathbf{I}}{dt} = -A\mathbf{R}, \tag{11}$$

where

$$\mathbf{R} = \begin{bmatrix} R_0 \\ R_1 \\ \vdots \\ R_N \end{bmatrix} \quad \mathbf{I} = \begin{bmatrix} I_0 \\ I_1 \\ \vdots \\ I_N \end{bmatrix} \quad A = \begin{bmatrix} a_0 & b & & & \\ b & a_1 & b & & \\ & \ddots & \ddots & \ddots & \\ & & b & a_N & \end{bmatrix}. \tag{12}$$

These equations of motion can be solved with a variety of numerical techniques, such as split-operators methods, finite-difference time-domain (FDTD) methods and the Leapfrog method. Here, we apply the Leapfrog method, which is a symplectic integrator technique that conserves the energy of a system and is fully reversible. For the TDSE, the Leapfrog preserves state normalization:

$$\frac{d(\mathbf{R^T R} + \mathbf{I^T I})}{dt} = \frac{d(|\psi(x,t)|)}{dt} = 0. \tag{13}$$

The Leapfrog techniques evolves the state one discrete time step at a time from the initial conditions by

$$\mathbf{R}_{1/2} = \mathbf{R}_0 + A\mathbf{I}_0 \frac{\Delta t}{2} \tag{14a}$$

$$\mathbf{I}_1 = \mathbf{I}_0 - A\mathbf{R}_{1/2} \Delta t \tag{14b}$$

$$\mathbf{R}_1 = \mathbf{R}_{1/2} - A\mathbf{I}_1 \frac{\Delta t}{2}. \tag{14c}$$

The von Neumann stability condition dictates that

$$\Delta t < \lambda h^2, \tag{15}$$

where $0 < \lambda < 1$ and $\lambda$ depends on the potential $V$. Here, we use $\lambda = 1/2$ as an appropriate value for $\lambda$ such that $dt = 0.5h^2$. Note that $h$ refers to the size of the spatial step size, not Planck's constant.

For all wave functions, we define the initial condition to be a Gaussian wave packet:

$$\psi(x,0) = (\sigma\sqrt{\pi})^{-1/2} \exp\left[ -\frac{(x-x_0)^2}{2\sigma^2} + ik_0 x \right], \tag{16}$$

where $x_0$ the center of Gaussian, $\sigma$ the width of Gaussian, and $k_0$ the initial average momentum. For all cases, we set $k = \omega_0 = m = 1$ for simplicity. Finally, we apply periodic boundary conditions $\psi_{N+1} = \psi_0$ and $\psi_{-1} = \psi_N$ to ensure the equations of motion in Eq. 11 are complete for all time steps.

## III. RESULTS

### A. Free Space and Matrix Solver Considerations

First, we consider the potential $V(x,t) = 0$ for a particle in free space with initial Gaussian parameters $x_0 = -5$, $\sigma = 0.5$, and $k_0 = 5$. We use $N = 1000$ discrete space points ranging from $-10$ to 10 in atomic units. Simulating $15,000$ time steps demonstrates the wave packet moving rightwards in space and looping back around as it goes through the boundary, confirming that the boundary conditions work as expected (Fig. 1). Dispersion is also observed as the wave packet spreads out over time.

To solve the equations of motion from Eq. 11, it is important to consider for large $N$, most matrix elements from Eq. 12 are zero. Instead of using the full matrix for solving the equations of motion, two efficient alternatives are examined. First, we examine a sparse matrix solver (SciPy's sparse csr_matrix) that reduces the memory requirements from $O(n^2)$ to $O(Tn)$ and the computational requirements from $O(n^3)$ to $O(Tn^2)$ for T average entries per column. Then, we examine an array slicing method that only iterates through the required values of the matrix to solve the equations of motion. We compare the full matrix, sparse matrix, and matrix slicing approaches for several numbers of space discretization points, as summarized in Tab. I. The matrix slicing is around 2.4 times faster than the sparse method, and both the slicing and sparse vastly outperform full matrix multiplication. The slicing method may outperform the sparse method because the matrix slicing for

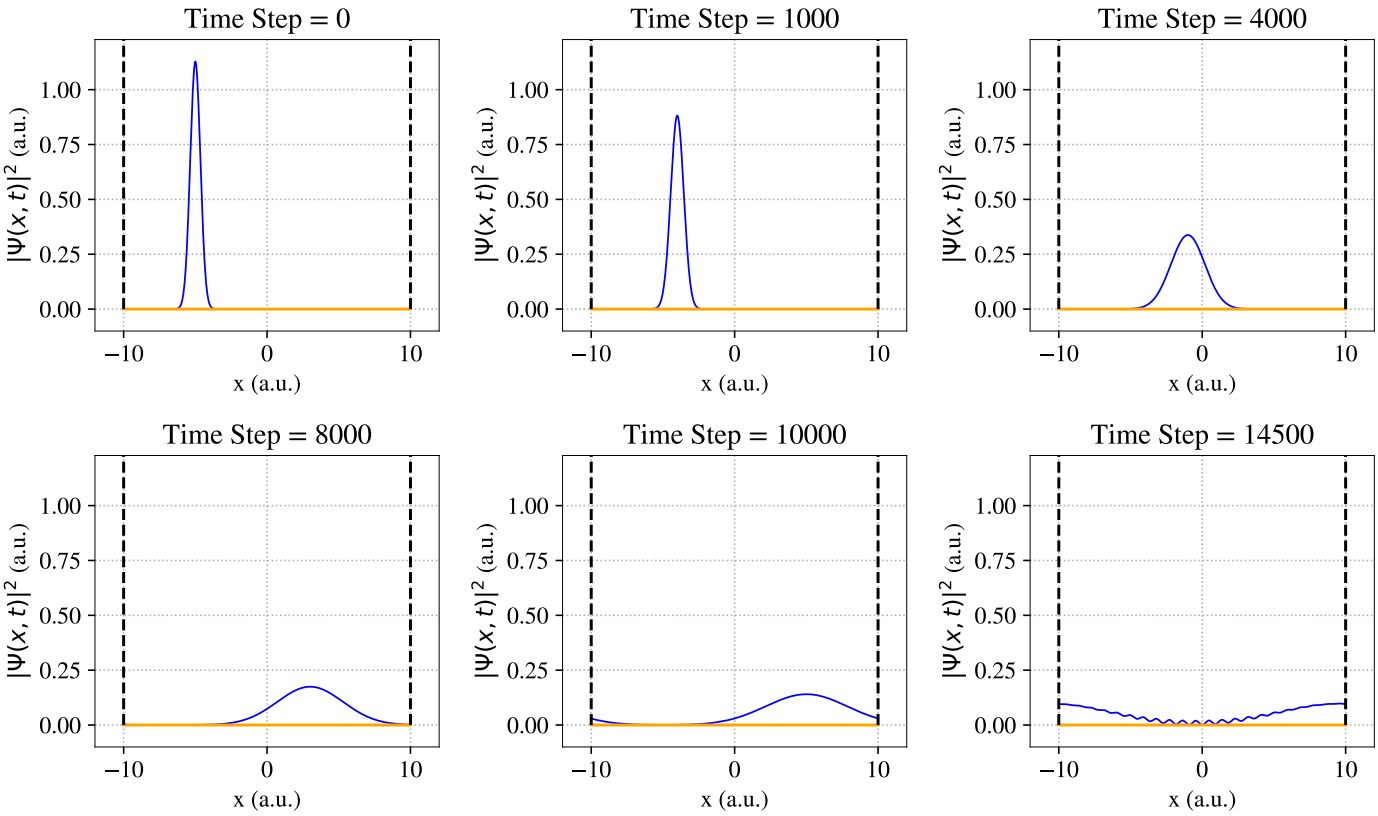


Figure 1. Evolution of the wave function in free space showing spreading of the wave function. The dashed black lines illustrate the bounds of the space points used in the calculation. We can observe that the wave packet exhibits dispersion and that the boundary conditions work as expected. Towards the end, the function becomes less smooth.

the matrix in 12 eliminates all zeros and is highly vectorized. Due to the superior performance, the slicing method is used for the remainder of the simulations in this paper.

Table I. Summary of timing results for solving the wave packet in free space over 15,000 time steps using different matrix solving methods. All times are in seconds. Three samples were taken for each method and averaged. The times for N=3,000 and N=10,000 for the full matrix method were omitted due to slow computation times. The results demonstrate that both sparse matrix multiplication and matrix slicing scale well with larger space discretization. This was done on an Intel Core i7 10700k with 32GB 3600MHz RAM.

| | | **Method** | | |
|---|---|---|---|---|
| | | Full Matrix | Sparse Matrix | Matrix Slicing |
| **N** | 1000 | 34.2 | 1.31 | 0.50 |
| | 2000 | 164.0 | 1.52 | 0.64 |
| | 3000 | N/A | 1.89 | 0.84 |
| | 10000 | N/A | 4.09 | 1.80 |

### B. Harmonic Oscillator

We then consider the potential $V(x,t) = \frac{1}{2}x^2$ with an initial Gaussian parameters $x_0 = -5$, $\sigma = 0.5$, and $k_0 = 0$.

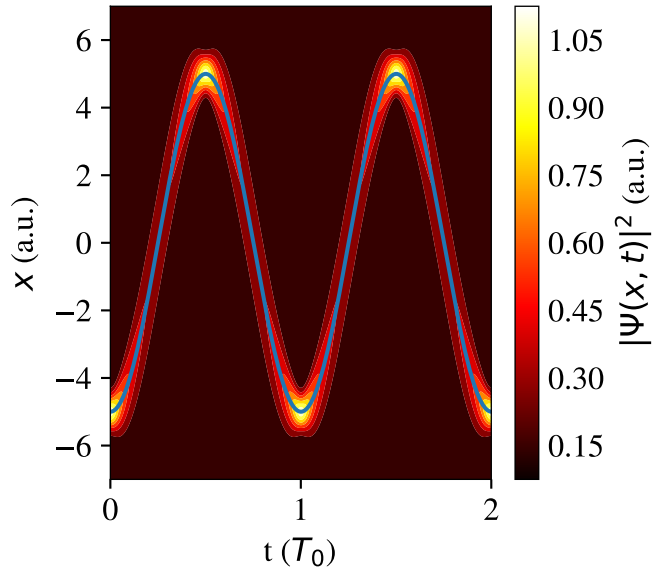


Figure 2. Probability density of wave function in harmonic oscillator over two periods, demonstrating oscillatory motion from $x = -5$ to $x = 5$. The blue line shows the position expectation value, $\langle x \rangle$.

We use $N = 1000$ discrete space points ranging from $-10$ to 10 in atomic units. Simulating two periods demonstrates oscillatory motion across the well as expected (Fig. 3). The probability density over time similarly demonstrates oscillatory motion (Fig. 2).

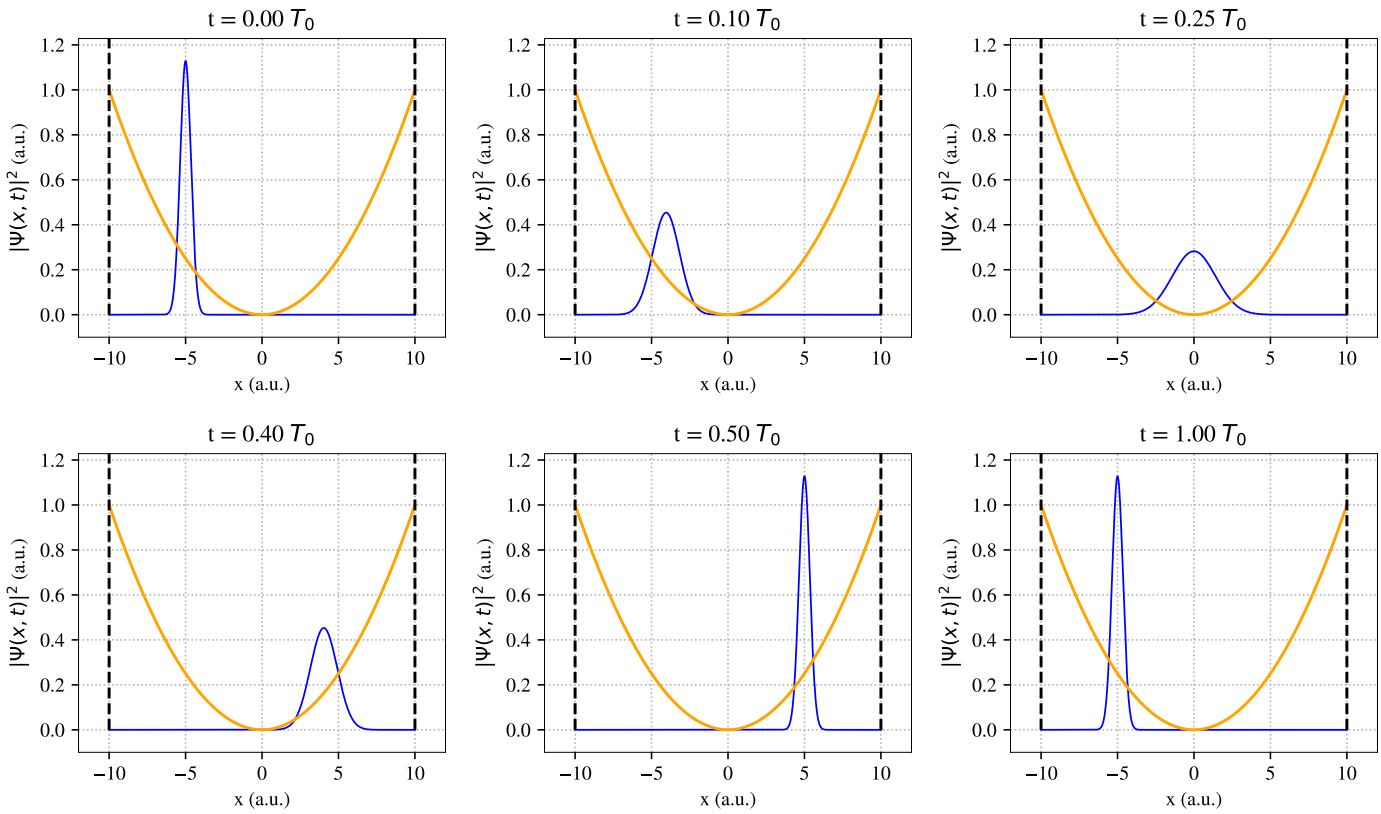


Figure 3. Evolution of the wave function over one period for the harmonic oscillator potential demonstrating oscillatory motion. The potential function has been scaled down for visibility. The dashed black lines illustrate the bounds of the space points used in the calculation.

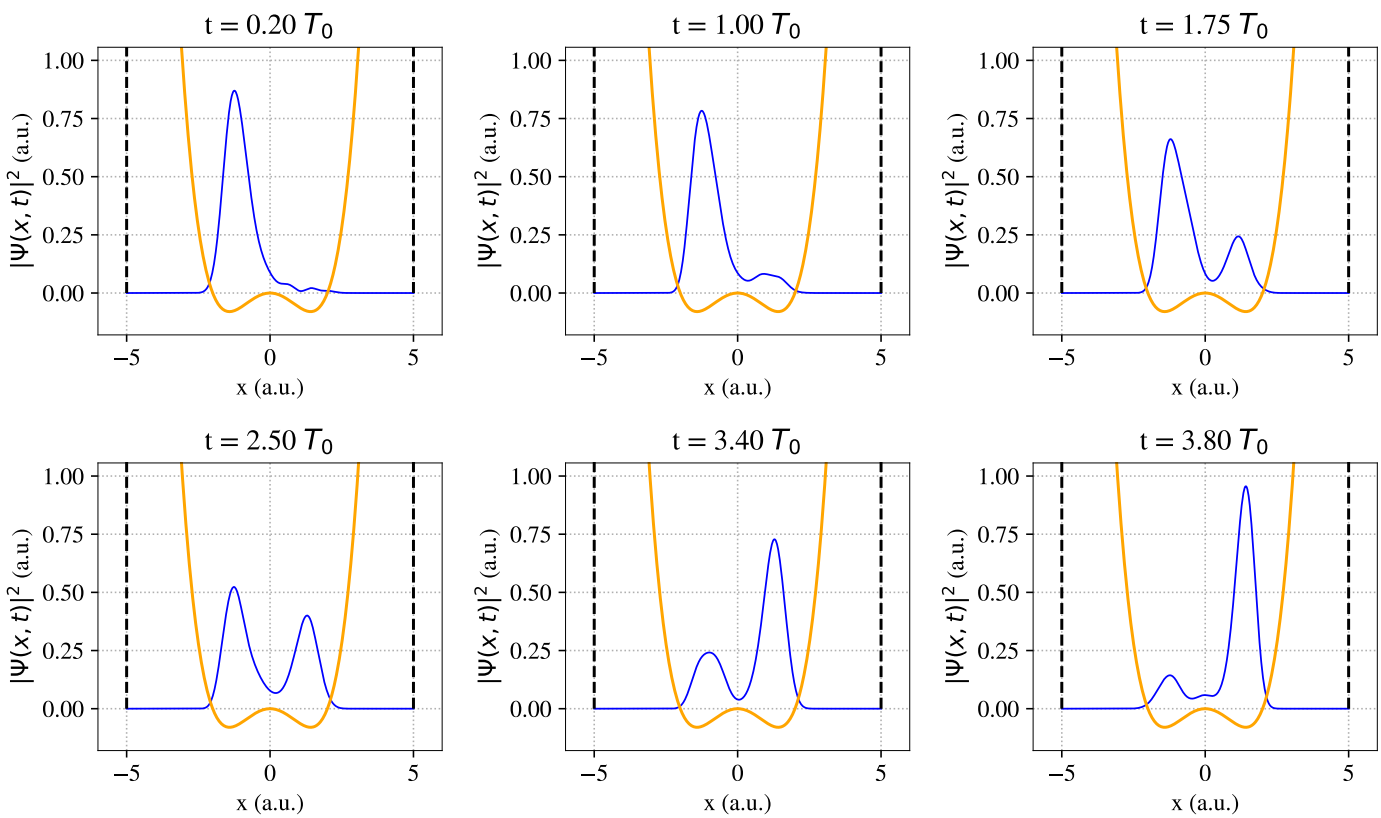


Figure 4. Evolution of the wave function in a double well potential for $a = 1$ and $b = 4$ over four nominal periods, demonstrating quantum tunneling across four nominal periods. Note that the potential function has been scaled down for visibility and the black dashed line represents the bounds of the space points used in the calculation.

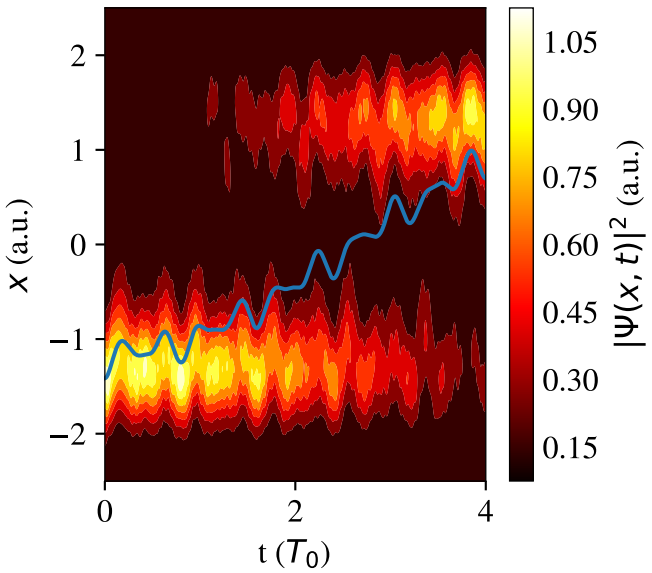


Figure 5. Probability density of wave function in double well potential for $a = 1$ and $b = 4$ over four nominal periods, demonstrating oscillatory quantum tunneling between the two wells. The blue line shows the position expectation value, $\langle x \rangle$.

Using these results, we can verify that the Virial Theorem is satisfied by considering the expectation value of the kinetic energy $\langle T \rangle$ and the expectation value of the potential energy $\langle V \rangle$ over any integer number of periods for time averaging. The Virial theorem states that $2\langle T \rangle = n\langle V \rangle$ where $n = 2$ for this specific problem. In turn, we expect $\langle T \rangle = \langle V \rangle$. We find the expectation value of the kinetic energy from Eq. 7 using a simple differences method for calculating the derivative of the wave function (NumPy's diff) and Simpson's integration method for the integral (SciPy's integrate simpson) to give $\langle T \rangle = 6.79$. We then find the expectation value of the potential energy from Eq. 8 using the same Simpson integration method to give $\langle T \rangle = 6.77$. This confirms $\langle T \rangle \cong \langle V \rangle$ within 0.3% accuracy which could be improved with more space points, and possibly other numerical differentiation and integration techniques.

### C. Double-well Potential

Finally, we consider the double-well potential $V(x,t) = ax^4 - bx^2$ with an initial Gaussian parameters $x_0 = -\sqrt{2}$, $\sigma = 0.5$, and $k_0 = 0$ such that the Gaussian starts in the left well. We begin by considering $a = 1$ and $b = 4$. We use $N = 500$ discrete space points ranging from $-5$ to 5 in atomic units. Simulating four nominal periods demonstrates quantum tunneling, as the wave packet probability distribution shifts back and forth between the two potential wells (Fig. 4)

This tunneling effect is clearly shown with a probability density distribution, showing how the expectation value $\langle x \rangle$ shifts between wells (Fig. 5).

We then investigate how changing the $a$ and $b$ parameters affect the quantum tunneling rates, or how rapidly the expectation value shifts between the two wells. It is more convenient to consider how $a/b$ changes the quantum tunneling rates. As $a/b$ increases, the outside wells steepen, and the inside hill shrinks, allowing the particle to pass more easily between wells, resulting in a faster quantum tunneling rate. Similarly, as $a/b$ decreases, the outside wells shrink, and the inside hill steepens, making it less likely for the particle to pass between the wells, resulting in a slower quantum tunneling rate. This is clearly shown in Fig. 6 and Fig. 8 for $a = 1$ and $b = 2$, and in Fig. 7 and Fig. 9 for $a = 1$ and $b = 8$.

## IV. CONCLUSION

Using space discretization and the Leapfrog technique, we solved the TDSE for free space, the harmonic oscillator and the double-well potential with the expected behaviour in all cases. The free space potential demonstrated dispersion over time, the harmonic oscillator demonstrated oscillatory motion across the potential well, and the double-well potential demonstrated periodic quantum tunneling across the two wells. We demonstrated that matrix slicing and sparse matrix multiplication vastly outperform full matrix multiplication for solving the equations of motion, and that slicing is around 2.4 times faster than the sparse method. The Virial theorem was verified within 0.3% for the harmonic oscillator using numerical differentiation and integration techniques. For the double-well potential, we showed that a larger $a/b$ ratio results in a higher rate of tunneling. Overall, we demonstrated the success of applying the space discretized Leapfrog technique to solving the TDSE.

Further work could be done by applying these methods to more complex potentials, such as the potentials of electrons in molecules. It could also be expanded to investigate different Hamiltonians such as time-dependent laser pulses, electric dipoles, or magnetic dipoles. Different numerical methods such as the split-operators method or FDTD method could be implemented and compared for performance and accuracy.

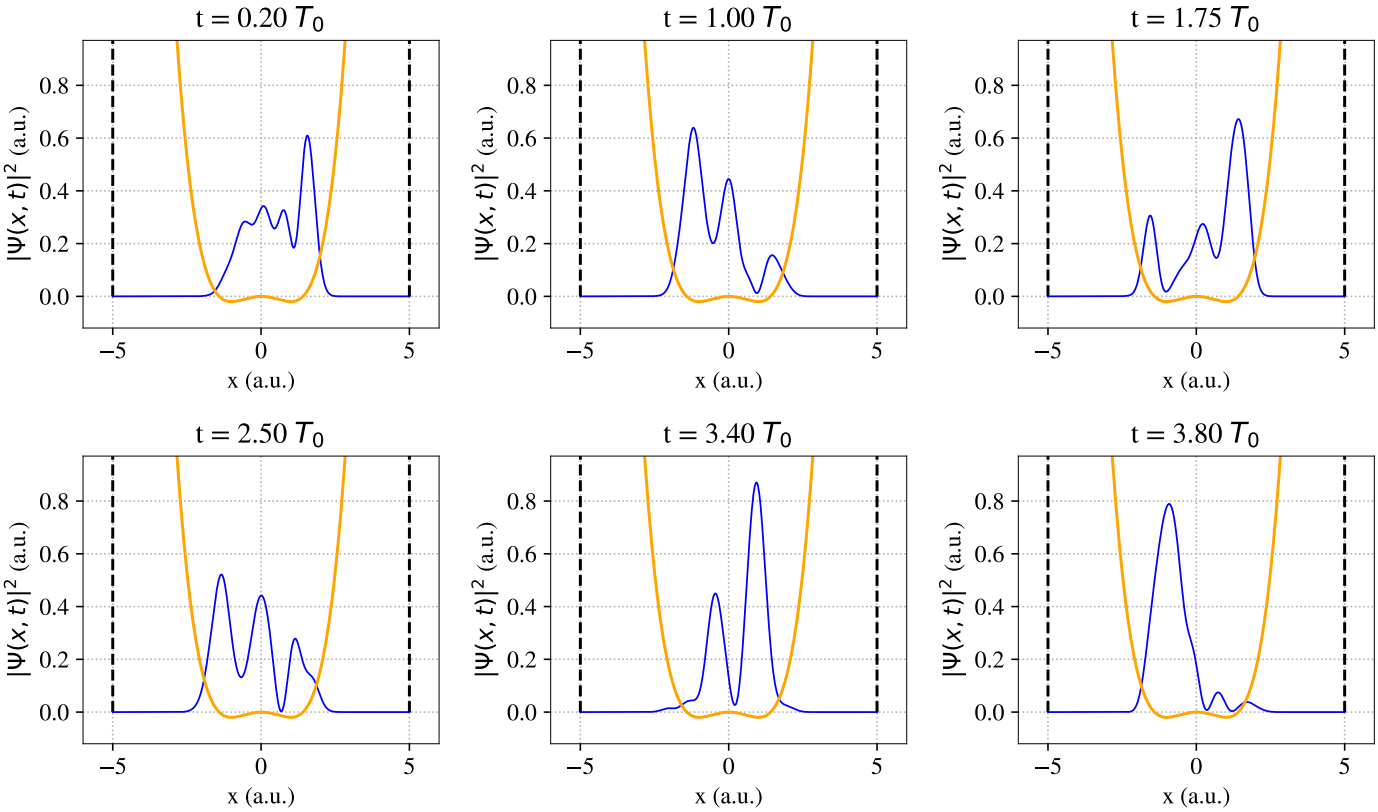


Figure 6. Evolution of the wave function in a double well potential for $a = 1$ and $b = 2$ over four nominal periods. Compared with the base case of $a = 1$ and $b = 4$, we observe a faster quantum tunneling rate because of the smaller potential barrier separating the two wells.

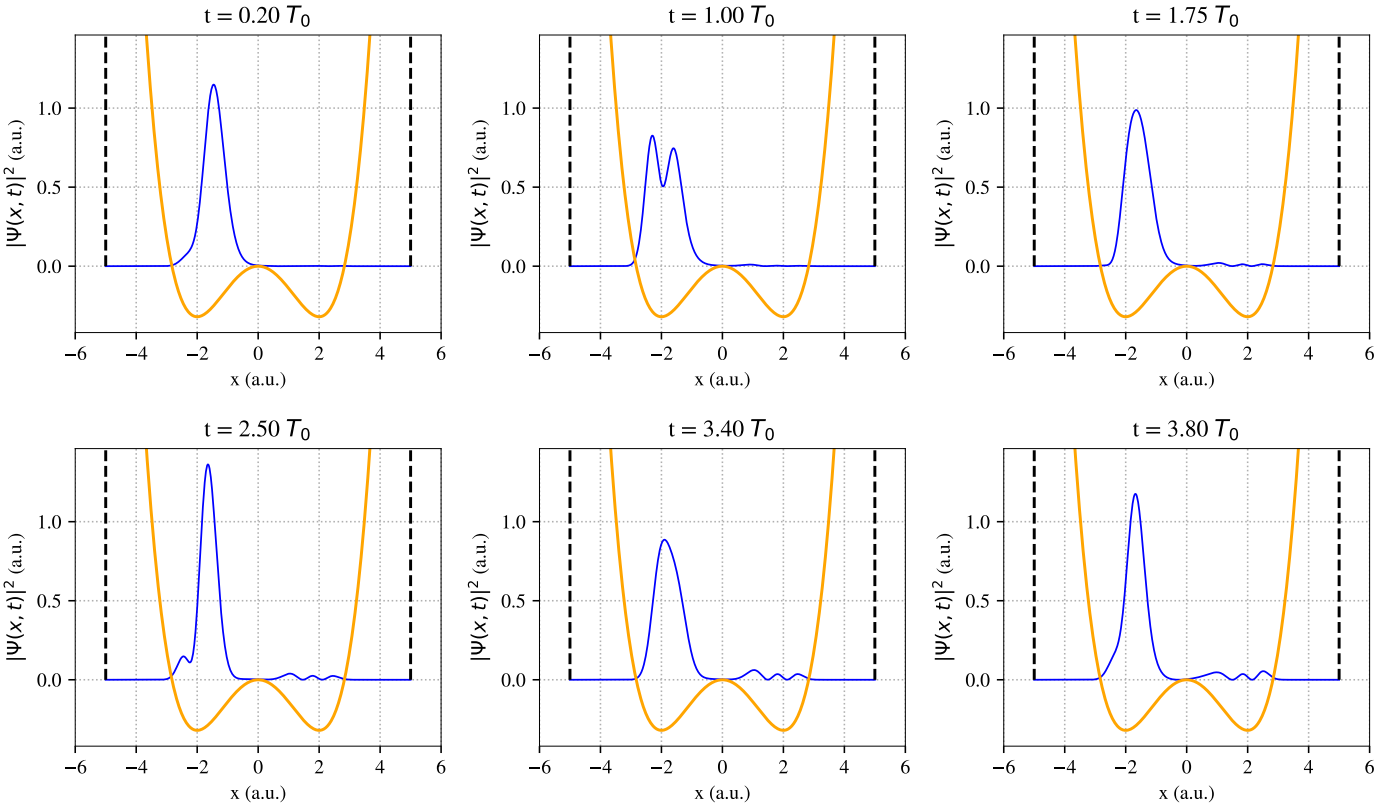


Figure 7. Evolution of the wave function in a double well potential for $a = 1$ and $b = 8$ over four nominal periods. Compared with the base case of $a = 1$ and $b = 4$, we observe a slower quantum tunneling rate because of the larger potential barrier separating the two wells.

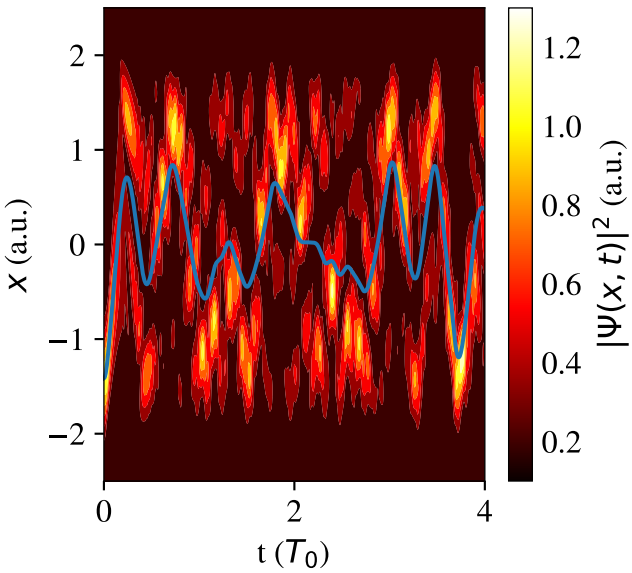


Figure 8. Probability density of wave function in double well potential for $a = 1$ and $b = 2$ over four nominal periods. Compared with the base case of $a = 1$ and $b = 4$, we observe a faster quantum tunneling rate because of the smaller potential barrier separating the two wells. The blue line shows the position expectation value, $\langle x \rangle$.

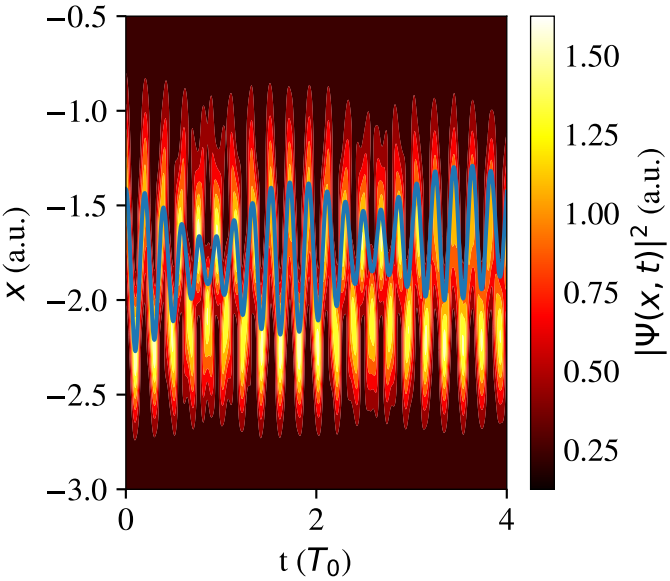


Figure 9. Probability density of wave function in double well potential for $a = 1$ and $b = 8$ over four nominal periods. Compared with the base case of $a = 1$ and $b = 4$, we observe a slower quantum tunneling rate because of the larger potential barrier separating the two wells. The blue line shows the position expectation value, $\langle x \rangle$.